A triple resonance hyperfine sublevel correlation experiment for assignment of electron-nuclear double resonance lines

Alexey Potapov, Boris Epel, and Daniella Goldfarb

Citation: The Journal of Chemical Physics **128**, 052320 (2008); doi: 10.1063/1.2833584
View online: http://dx.doi.org/10.1063/1.2833584
View Table of Contents: http://scitation.aip.org/content/aip/journal/jcp/128/5?ver=pdfcov
Published by the AIP Publishing

A triple resonance hyperfine sublevel correlation experiment for assignment of electron-nuclear double resonance lines

Alexey Potapov,[1] Boris Epel,[2] and Daniella Goldfarb[1,a)]
[1]*Chemical Physics Department, Weizmann Institute of Science, Rehovot 76100, Israel*
[2]*Department of Radiation and Cellular Oncology, MC1105 The University of Chicago Medical Center, Chicago, Illinois 60637, USA*

(Received 22 October 2007; accepted 17 December 2007; published online 6 February 2008)

A new, triple resonance, pulse electron paramagnetic resonance (EPR) sequence is described. It provides spin links between forbidden electron spin transitions ($\Delta M_S = \pm 1$, $\Delta M_I \neq 0$) and allowed nuclear spin transitions ($\Delta M_I = \pm 1$), thus, facilitating the assignment of nuclear frequencies to their respective electron spin manifolds and paramagnetic centers. It also yields the relative signs of the hyperfine couplings of the different nuclei. The technique is based on the combination of electron-nuclear double resonance (ENDOR) and electron-electron double resonance (ELDOR)–detected NMR experiments in a way similar to the TRIPLE experiment. The feasibility and the information content of the method are demonstrated first on a single crystal of Cu-doped L-histidine and then on a frozen solution of a Cu-histidine complex. © *2008 American Institute of Physics*. [DOI: 10.1063/1.2833584]

INTRODUCTION

Structural properties of paramagnetic systems are often derived from hyperfine and nuclear quadrupole interactions of nuclear spins coupled to the electron spin. These interactions are usually small and yield splittings that are not resolved in the electron paramagnetic resonance (EPR) spectrum, especially in the solid state where the EPR spectrum is inhomogeneously broadened. Therefore, these interactions are usually determined from the NMR frequencies of the coupled nuclei. The energy level diagram for the most simple system, consisting of one electron spin, $S=1/2$, coupled to one nuclear spin $I=1/2$, is shown in Fig. 1. There are four EPR transitions, two allowed transitions ($\Delta M_S = \pm 1$, $\Delta M_I = 0$) denoted by a and two forbidden transitions ($\Delta M_S = \pm 1$, $\Delta M_I \neq 0$) denoted by f. In addition, there are two allowed NMR transitions, referred to as $a(n)$.

For an electron spin $S=1/2$ coupled to a nuclear spin I, the first order nuclear frequencies are

$$\nu_{\alpha,\beta}(M_I) = |-\nu_I \pm A/2 + P(2M_I - 1)|, \quad (1)$$

where α and β denote $M_S = \pm 1/2$, respectively, ν_I is the nuclear Larmor frequency, A is the hyperfine coupling, and P is the nuclear quadrupole coupling for nuclei with $I > 1/2$. A and P are functions of the principal values of the hyperfine (A_{xx}, A_{yy}, A_{zz}) and nuclear quadrupolar (P_{xx}, P_{yy}, P_{zz}) tensors and of the orientation of their principal axes systems with respect to the external magnetic field. In general, for each M_S manifold (α or β) there are $2I$ allowed NMR transitions. For $I=1/2$, there are only two, ν_α and ν_β. The frequency difference between the allowed and forbidden EPR transitions give the nuclear frequencies.

The most common pulse EPR techniques designed to measure the NMR frequencies of nuclei coupled to unpaired electron(s) are the electron nuclear double resonance (ENDOR) and electron spin echo envelope modulation (ESEEM) techniques. The ENDOR techniques comprise pulse sequences with microwave (MW) pulses to induce allowed EPR transitions and radio frequency (RF) pulses for the allowed NMR transitions. In contrast, the ESEEM sequences involve only MW pulses, which generate echoes and rely on the simultaneous excitation of allowed and forbidden EPR transitions. The decay of the produced echo is, in turn, modulated with the nuclear frequencies and Fourier transform yields the desired spectrum. Because ENDOR and ESEEM measurements generate only positive frequencies, it is usually impossible to determine which of the NMR frequencies correspond to ν_α and which to ν_β. Therefore, the sign of the hyperfine coupling remains unknown.

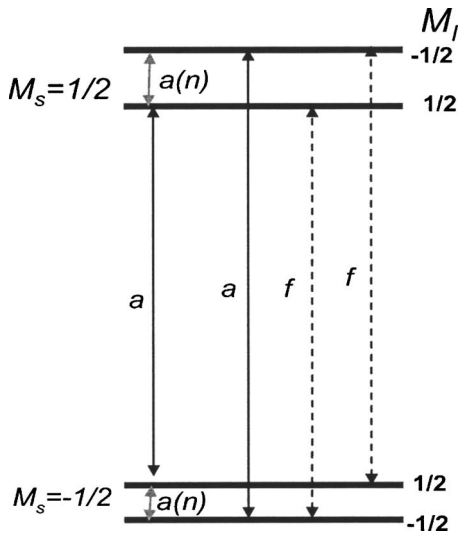

FIG. 1. Energy level diagram for $S=1/2$, $I=1/2$, marking the EPR allowed (a) and forbidden (f) transitions and the allowed NMR transitions [$a(n)$].

a)Electronic mail: daniella.goldfarb@weizmann.ac.il.

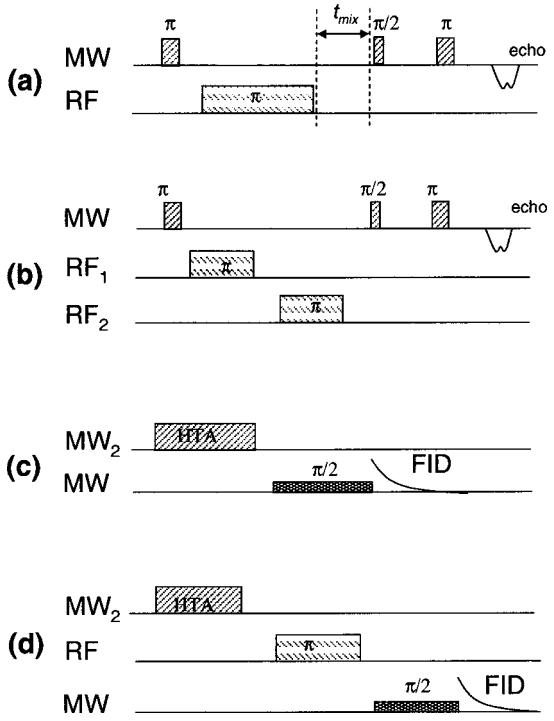

FIG. 2. The pulse sequences employed in this work (a) Davies ENDOR. t_{mix} is usually set to the minimum possible and the spectrum is registered by measuring the echo intensity as a function of the RF. (b) TRIPLE, (c) ELDOR-detected NMR, and (d) THYCOS.

The spectra generated by the ENDOR and ESEEM techniques are often not straightforward to interpret owing to lack of resolution because of overlapping signals from different nuclei and the presence of multiple paramagnetic centers. Therefore, methods which provide correlations between signals and resolve them into two dimensions (2D) are most useful. The best known and most widely applied correlation experiment in EPR is the hyperfine-sublevel correlation technique (HYSCORE).[1] It is an ESEEM based 2D experiment that correlates nuclear frequencies belonging to different electron spin manifolds, namely, cross peaks appear at (ν_α, ν_β) and (ν_β, ν_α).

The earliest ENDOR related correlation spectroscopic technique is TRIPLE, first designed as a continuous wave (cw) experiment, which correlates NMR transitions belonging to the same M_S manifold and thereby providing the relative signs of the hyperfine splittings.[2] It is called TRIPLE because it uses three irradiation fields, one MW and two RF fields. The pulse version of TRIPLE is based on the standard Davies ENDOR pulse sequence, shown in Fig. 2(a), with an additional RF π-pulse applied during the mixing time interval [Fig. 2(b)].[3] In this experiment RF_1 is set to one of the ENDOR transitions and the spectrum is obtained by recording the echo intensity as a function of RF_2. The difference between this spectrum and the ENDOR spectrum generates the so-called "difference" TRIPLE spectrum, which shows only ENDOR lines belonging to the same M_S manifold as the nuclear transition selected by RF_1. Pulse TRIPLE has also been extended to two dimensions where both RF_1 and RF_2 are swept.[4,5] When applied to disordered systems, such as frozen solutions, the 2D experiment can provide the relative orientation of the hyperfine tensors of different nuclei.[5] Other ENDOR based correlation experiments that correlate the hyperfine coupling and the NMR frequencies of a particular nucleus are 2D Mims,[6] hyperfine-selective ENDOR,[7] Fourier-transform hyperfine spectroscopy,[8] and hyperfine-correlated ENDOR.[9] A common feature of these techniques is that the manipulation of the spin system is done via the allowed electron-spin and nuclear-spin transitions. In contrast, in the ESEEM-ENDOR experiment, nuclear frequencies arising from the excitation of allowed nuclear transitions are correlated with ESEEM frequencies, arising from the excitation of forbidden electron transitions.[10]

ELDOR-detected NMR,[11] shown in Fig. 2(c), is an alternative approach for measuring the nuclear frequencies. In this experiment, a high turning angle (HTA) MW pulse, with a frequency ν_{HTA}, burns a pattern of holes in the inhomogeneous EPR line shape arising from excitation of allowed and forbidden EPR transitions. This pattern is then detected by the intensity of the free induction decay (FID) produced by the application of a weak MW pulse at a different frequency ν_{det}. In practice, the spectrum is recorded by sweeping ν_{HTA} and holding ν_{det} constant. The hole appearing at $\Delta\nu = \nu_{HTA} - \nu_{det} = 0$ corresponds to the allowed EPR transitions, while excitation of forbidden EPR transition produces holes at $\Delta\nu = \nu_{HTA} - \nu_{det} \neq 0$, corresponding to the nuclear frequencies. These, as in the case of three-pulse ESEEM, include single quantum and multiple quantum nuclear transition frequencies. The major drawback of this experiment is its low resolution because the width of the hole that can be burnt in the EPR spectrum is determined by the electron spin phase memory time T_m,[12] which is relatively short and, therefore, this experiment is not very popular. It has recently attracted some interest when recorded at frequencies higher than *X*-band (~9.5 GHz), where the nuclear frequencies are high enough and reasonably removed from the central hole.[13,14] Although the ENDOR technique produces spectra with much better resolution than ELDOR-detected NMR, there are instances where the latter may be advantageous. For example, when the expensive ENDOR hardware is not available, or when it is not possible to create a large enough RF field in a large frequency range. In addition, when the forbidden transitions are pronounced, ELDOR-detected NMR may have better S/N.

In this work, we present a new correlation method that combines the ELDOR-detected NMR and ENDOR sequences to generate a correlation experiment with an information content similar to pulse TRIPLE. We refer to this experiment as triple resonance hyperfine sublevel correlation spectroscopy (THYCOS) [Fig. 2(d)]. The TRIPLE experiment starts with a Davies ENDOR sequence, where a selective MW pulse inverts the populations of one of the allowed EPR transitions ($\Delta M_S = \pm 1$) and a following selective RF pulse inverts the population of a connected allowed NMR transition ($\Delta M_I = \pm 1$). In the THYCOS experiment, the nonequilibrium population state obtained by the application of these two pulses is achieved in single step by a HTA pulse that selectively inverts the population of a forbidden transition ($\Delta M_S = \pm 1$, $\Delta M_I \neq 0$). The presence of an anisotropic hyperfine interaction or a nuclear quadrupole interaction

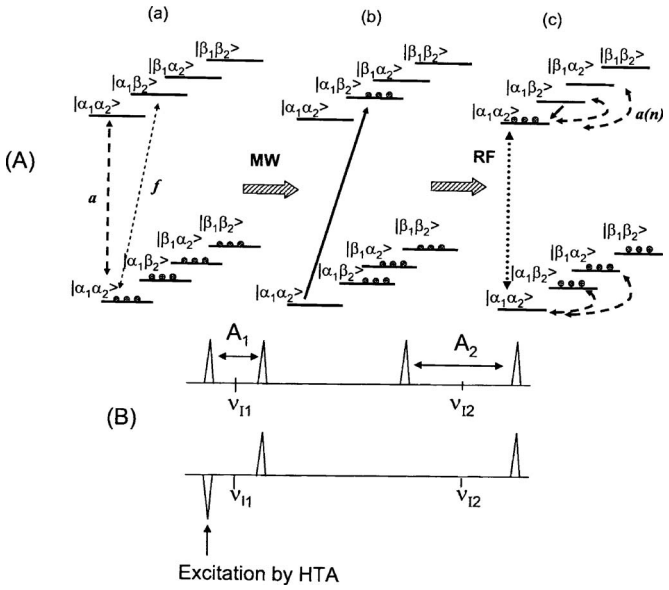

FIG. 3. (A) Qualitative explanation of the THYCOS experiment for an electron spin $S=1/2$ coupled to two nuclei with spins $I_1=1/2$ and $I_2=1/2$. The bottom levels corresponds to the electron spin β and the top levels to the electron spin α manifolds. The states specified on the figure correspond only to the nuclear spin state. (a) The populations at thermal equilibrium. Dashed arrows represent the allowed (a) and forbidden (f) transitions involved. (b) Populations after applying the HTA pulse to the forbidden transition indicated by the solid arrow. (c) Populations after applying a pulse to one of the allowed nuclear transition (solid arrow). The dotted arrow corresponds the allowed transition being detected. Dashed circled arrows point to other possible allowed nuclear transitions [$a(n)$] that will generate a change in the intensity of the detected signal. (B) The corresponding schematic ENDOR (top) and THYCOS (bottom) spectra. Arrow indicates the line excited by the HTA pulse.

make such an excitation possible. The evolution of the energy level populations in the THYCOS experiment for $S=1/2$, coupled to two nuclear spins with $I_1=I_2=1/2$, is shown in Fig. 3(A). A HTA pulse at ν_{HTA}, excites one of the forbidden transition and flips the electron spins from the α to the β manifold with a simultaneous flip of the nuclear spin of I_1. Next, the RF pulse moves populations within the nuclear subsystem. Two cases can be differentiated: (i) the RF matches nuclear transitions within the β-electron spin manifold and the intensity of the FID following a selective MW π pulse on the allowed EPR transition will increase. (ii) The RF matches transitions within the α-electron spin manifold and the FID intensity is reduced. The HTA pulse can, in principle, also excite transitions with $\Delta M_I=\pm 2$ and higher.

The THYCOS sequence can be implemented in several versions. The most general one is a 2D experiment where both ν_{HTA} and the RF are swept. Alternatively, 1D experiments can be performed with either the MW or RF frequencies fixed on one of the nuclear transitions while the other is swept. We find it advantageous to fix ν_{HTA} and sweep the RF because this approach yields a resolved ENDOR subspectrum. Furthermore, it does not require subtraction of the spectrum recorded without the HTA pulse from that obtained with the HTA pulse because without the HTA pulse there are no signals. In this version, the spectrum shows all the NMR transitions in the opposite manifold of that excited by the HTA pulse [Fig. 3(B)]. Here, we demonstrate the feasibility of the experiment using a W-band spectrometer (94.9 GHz) on a single crystal of Cu(II)-doped L-histidine and on a frozen aqueous solution of a Cu(II)-L-histidine (CuHis) complex. The single crystal example demonstrates the resolving power of the method in the case of signals arising from different species, showing how all ^{1}H signals can be assigned to their respective electron spin manifolds and how the sign of the ^{63,65}Cu hyperfine coupling can be determined. The example of the frozen solution shows the feasibility of the experiment when applied to an orientationally disordered sample, where it can resolve overlapping subpowder patterns and, thereby, demonstrate the THYCOS experiment's applicability to a wide range of systems.

EXPERIMENTAL

Sample preparation

The procedure for the single crystal sample preparation was described elsewhere.[15] The sample that was used for the measurements had an irregular shape and consisted of one large crystal and several smaller satellite crystals with different orientations of the crystallographic axis.

The preparation of Cu(II)-bis-L-histidine complex (CuHis) solution followed the procedure given in Ref. 16. The complex was prepared in 20 mM HEPES buffer pH 7.3 and glycerol was used as glass-forming agent. A mixture of 1:1 D_2O and fully deuterated glycerol was used to remove signals from solvent and exchangeable protons. A solution containing 2 mM $CuSO_4$ and 10 mM of L-histidine was prepared by mixing the components, followed by incubation for 30 min at room temperature.

Spectroscopic measurements

All measurements were performed at W-band (94.9 GHz) on a homebuilt spectrometer[17] with an upgraded microwave bridge featuring two channels with independent control of frequency and power. The spectrometer is equipped with two MW sources at 7.3 GHz: Herley CTI XS-7311 and ADF4113. Herley is used as the main source (used also as a reference for the detection system) because of its better phase noise characteristics. The ADF4113 source is used for the HTA pulse channel. The spectral resolution of the latter is 20 kHz, which gives an actual resolution of 260 kHz after the 13-fold multiplication to yield the final 94.9 GHz frequency. The control of both sources is implemented in the spectrometer control program SpecMan4EPR.[18]

The temperature for all measurements was 8.5 K, unless stated otherwise. The echo-detected (ED) EPR spectra were recorded with the $\pi/2-\tau-\pi-\tau-echo$ sequence, the lengths of the $\pi/2$ and π pulses were 100 and 200 ns, respectively. For Davies ENDOR, the inversion MW π pulse was 172 ns and the echo detection pulses were as above. The length of the RF pulse t_{RF} was chosen as a compromise between the resolution required for the single crystal narrow lines and the shortest possible pulse required for achieving the largest ENDOR effect. The length of 20 μs was set for all the experiments including THYCOS. The RF power level was kept constant giving π rotation for protons. For variable mixing

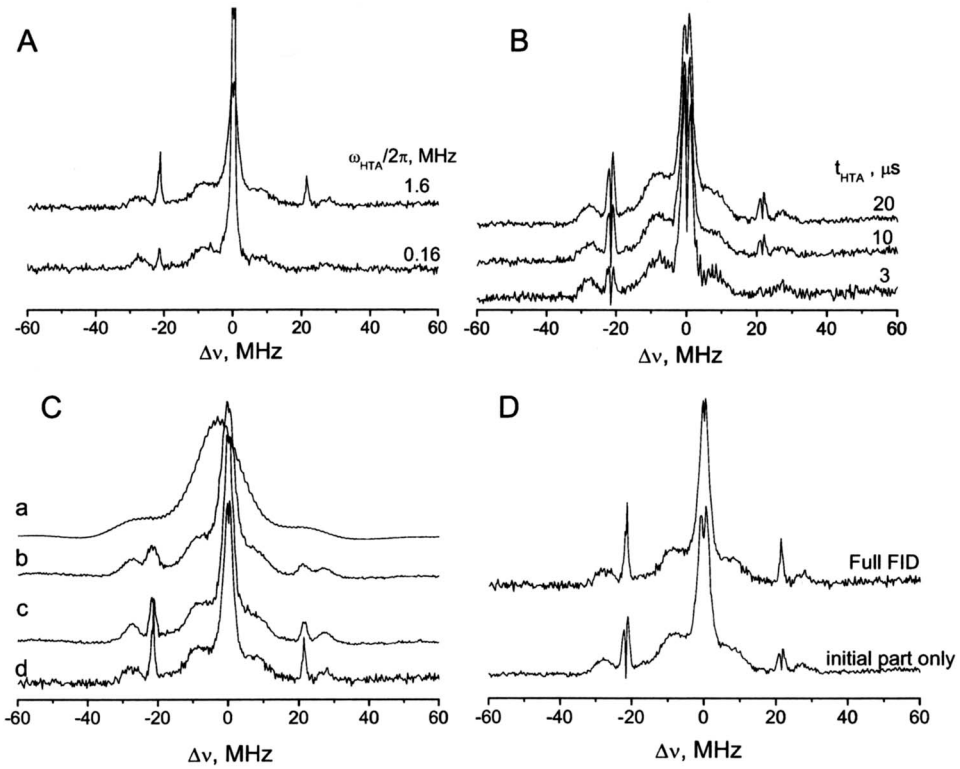

FIG. 4. Illustrations of the effect of the ELDOR-detected NMR experimental parameter setting on the spectrum of a frozen solution of CuHis. (A) The dependence of line intensities on the MW power: $\omega_{1\,det}/2\pi=0.08$ MHz, $t_{det}=3$ μs, $t_{HTA}=20$ μs, $\omega_{HTA}/2\pi=1.6$ and 0.16 MHz and (B) on the length of the HTA-pulse length t_{HTA}; $\omega_{1\,det}/2\pi=0.08$ MHz, $\omega_{1HTA}/2\pi=1.6$ MHz, $t_{det}=3$ μs, $t_{HTA}=3$, 10, and 20 μs. Here, the ELDOR-detected NMR spectra were normalized to the depth of the central hole. (C) Comparison of spectra acquired with spin echo and FID detections. (a) the echo is formed by $t_{\pi/2}=20$ ns and $t_{\pi}=40$ ns; (b) $t_{\pi/2}=100$ ns, $t_{\pi}=200$ ns; and (c) $t_{\pi/2}=200$ ns, $t_{\pi}=400$ ns. (d) Detection by integration over the FID following $t_{det}=3$ μs. The smaller bandwidth results in more resolved lines. Conditions: $\omega_{1\,det}/2\pi=0.08$ MHz, $\omega_{1HTA}/2\pi=1.6$, $t_{HTA}=20$ μs. (D) The effect of the width of the FID. Integration over the entire FID removes the artifacts observed in incomplete integration. Parameters are the same as in [(C)(d)].

time (VMT) ENDOR, where an additional time interval t_{mix} is added after the RF pulse, a mixing interval of 1 ms was sufficient to observe the desired effect.[19,20]

The detection $\pi/2$-pulse t_{det} in the ELDOR-detected NMR was set to 3 μs based on phase memory time T_m measurements. T_m was ~1.4 and ~6.5 μs for the single crystal and frozen solution samples, respectively. The HTA pulse length t_{HTA} was 2 μs with a nominal flip angle of 4π for the allowed transition. These parameters were chosen as a compromise between resolution and sensitivity of the experiment. The number of points in the ELDOR-detected NMR spectra was the largest attainable with the given source resolution. The ENDOR and ELDOR-detected NMR spectra were collected using the random acquisition mode[21] with 30 shots accumulated for each point in a RF or ν_{HTA} setting. The total number of scans varied according to S/N required. All ELDOR-detected NMR spectra were multiplied by −1 for convenient presentation.

Settings for ELDOR-detected NMR

The adjustment of the experimental parameters for the ELDOR-detected NMR experiment is not straightforward. The experimental settings are determined by an optimal trade-off between resolution and sensitivity. The depth of the hole h burnt in an inhomogeneously broadened spectrum by a pulse consists of contributions from overlapping forbidden and allowed transitions, arising from different spin packets, according to[11]

$$h = 1 - I_a \cos(\beta_0 \sqrt{I_f}) - I_f \cos(\beta_0 \sqrt{I_a}).$$

I_a and I_f are the probabilities of the allowed and forbidden transitions, respectively, and β_0 is the nominal flip angle, $\beta_0=\omega_1 t_p/\hbar$, where $\omega_1=\gamma_e B_1$ and B_1 is the amplitude of the MW field. Thus, stronger and longer pulses produce deeper holes, as demonstrated in Figs. 4(A) and 4(B). On the other hand, the width of the hole depends on B_1, the pulse length t_p, and the phase memory time T_m. The narrowest possible hole, given by T_m^{-1}, can be achieved by the application of a weak pulse with a fixed flip angle of π such that $1/\omega_1 T_m \gg 1$, thereby, obtaining the best resolution.

Another important parameter in the ELDOR-detected NMR experiment is the detection of the burnt hole pattern. Possible ways are to detect the FID intensity (integration of the FID) created by a single long and weak pulse, as proposed in the original version of ELDOR-detected NMR experiment[11] and shown in Fig. 2(c), or the amplitude of a two-pulse echo. In both cases, pulses with the smallest possible bandwidth are desired; otherwise, the acquired spectrum is broadened. This, however, comes at the expense of S/N, therefore, in case of relatively broad lines, sensitivity may be gained by applying short pulses without compromising much in resolution. This is clearly shown in Fig. 4(C)(a)–4(C)(c), which compares ELDOR-detected NMR spectra recorded with echo-forming pulses of different durations. Improved resolution, again, at the expense of S/N, is obtained by FID detection, as shown in Fig. 4(C)(d). One important aspect of FID detection is the width of the integration window. Setting the window in a way that maximizes S/N may lead to artifacts because the shape of the FID may contain oscillatory signals appearing when the linewidth is smaller than the detection pulse bandwidth. This could be avoided by integrating over the whole FID that lasts for a time t_p, as shown in Fig. 4(D). This figure shows that a too

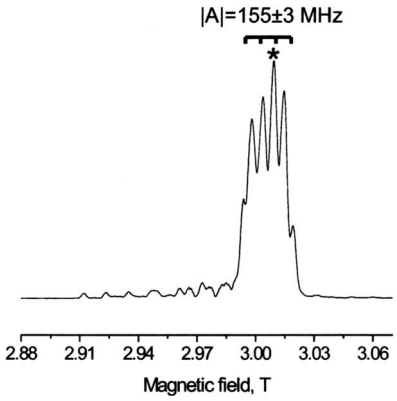

FIG. 5. ED-EPR spectrum of Cu(II)-doped L-histidine single crystal; * points to the field at which the ENDOR and ELDOR-detected NMR experiments were carried out.

short integration window leads to a "hole" in the middle of the peak at ± 21 MHz, which can be mistaken as a splitting.

The THYCOS sequence also involves a period after the HTA excitation during which the RF pulse is applied. The z-magnetization produced by the HTA pulse may be transferred by spectral diffusion processes or other magnetization transfer processes and, thereby, broadening the hole. We did not detect any observable broadening of the hole within 100 μs of evolution time (data not shown) in our samples. The phases of the two different MW sources in our setup are not locked relative to each other and any coherences created by the HTA pulse will be averaged to zero during data accumulation. Hence, the evolution period after the HTA-pulse in ELDOR-detected NMR can be shorter than T_m and phase cycling is not required.

RESULTS

Single crystal

The echo-detected (ED) EPR spectrum of a Cu-doped-L-histidine single crystal should exhibit two groups of lines belonging to two paramagnetic sites in the unit cell of the crystal.[22] The spectrum of the crystal, mounted at an arbitrary orientation, depicted in Fig. 5, shows a superposition of two overlapping quartets with relatively high intensities, which we attribute to the aforementioned sites. Additional lines with lower intensities are found as well and are attributed to small crystallites in the sample. The ^{63,65}Cu (^{63}Cu, 69%, g_n=1.484, $I=\frac{3}{2}$, and ^{65}Cu 31%, g_n=1.588, $I=\frac{3}{2}$) hyperfine splitting $|A_{\mathrm{Cu}}|$ of the major quartet is 155 ± 3 MHz. The splitting due to the different isotopes is not resolved. The magnetic field chosen for the experiment was set to the third line of the quartet, as shown in Fig. 5. For this field position, the ^{63,65}Cu lines in the ENDOR spectrum arises from $\Delta M_I = \pm 1$ transitions, specifically those corresponding to $M_I = \frac{3}{2} \leftrightarrow \frac{1}{2}$ and $M_I = \frac{1}{2} \leftrightarrow -\frac{1}{2}$ transitions (see Fig. 7). The latter is affected by the quadrupolar coupling of the ^{63,65}Cu nuclei only in the second order of perturbation theory, which allowed us to estimate [using Eq. (1)] that the ENDOR lines of the β and α electron spin manifolds of the major isotope

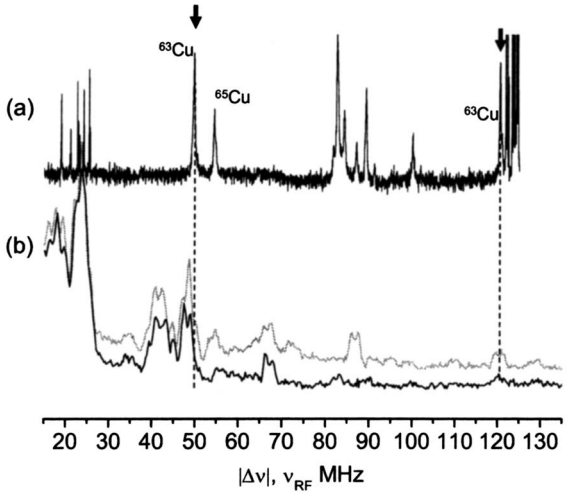

FIG. 6. (a) Davies ENDOR spectra of a Cu(II)-doped L-histidine single crystal, MW pulses 200 ns/100 ns/200 ns, t_{RF}=20 μs. (b) ELDOR-detected NMR spectra (t_{HTA}=3 μs and t_{det}=2 μs). Spectra with positive (gray) and negative (black) values of $\Delta\nu$ are superimposed on the Figure. The arrows mark the frequency of the HTA pulse in the THYCOS experiment.

^{63}Cu should appear at ~50 MHz and ~120 MHz, respectively, assuming $A_{\mathrm{Cu}}<0$.

The Davies ENDOR spectrum, recorded at the indicated field position, is shown in Fig. 6(a). It is complicated and consists of a number of groups of lines; those in the interval of 5–30 MHz belong to strongly coupled ^{14}N and weakly coupled ^{35}Cl nuclei, protons appear at 120–140 MHz (Ref. 23) and all the other lines are ^{63,65}Cu lines. Peaks of ^{63}Cu at 50 and 120 MHz are detected, as predicted, and are labeled with arrows on Fig. 6(a). One of the corresponding lines of ^{65}Cu is indicated as well. There are many other Cu lines in the ENDOR spectrum that correspond to the ^{63}Cu $M_I = \frac{3}{2} \leftrightarrow \frac{1}{2}$ transition, to ^{65}Cu lines and to other crystallites. Here, we focus only on the ^{63}Cu $m_I = \frac{1}{2} \leftrightarrow -\frac{1}{2}$ transitions of the major quartet.

The ELDOR-detected NMR spectrum is also shown in Fig. 6(b) and the positive and negative parts of the spectrum are superimposed. The ENDOR spectrum is considerably better resolved than the ELDOR-detected NMR spectrum, as expected. It is important to stress that the single crystal ELDOR-detected NMR spectrum lacks the symmetry around the center of the spectrum, $\Delta\nu$=0, that is often found in a frozen solutions. In frozen solutions the selectivity in the excitation of a particular M_I component by the HTA pulse is limited because of the inhomogeneous broadening. In contrast, in a single crystal, additional resolution is provided by the separation of the positive and negative sides, as illustrated in Fig. 6(b). When the detection is set to an allowed electron transition with $M_I = \frac{1}{2}$, forbidden transitions with frequencies smaller than the detection frequency (negative side, $\Delta\nu<0$) are from $M_I = \frac{3}{2} \leftrightarrow \frac{1}{2}$ in the α and β manifolds. Forbidden transitions with $\Delta\nu>0$, positive side, originate from the $M_I = \frac{1}{2} \leftrightarrow -\frac{1}{2}$ in α and β manifold (see Fig. 7). Selection of a different M_I component by the HTA pulse will give a different partitioning of the signals, as shown Fig. 7(b). Hence, lines corresponding to different M_I transitions appear

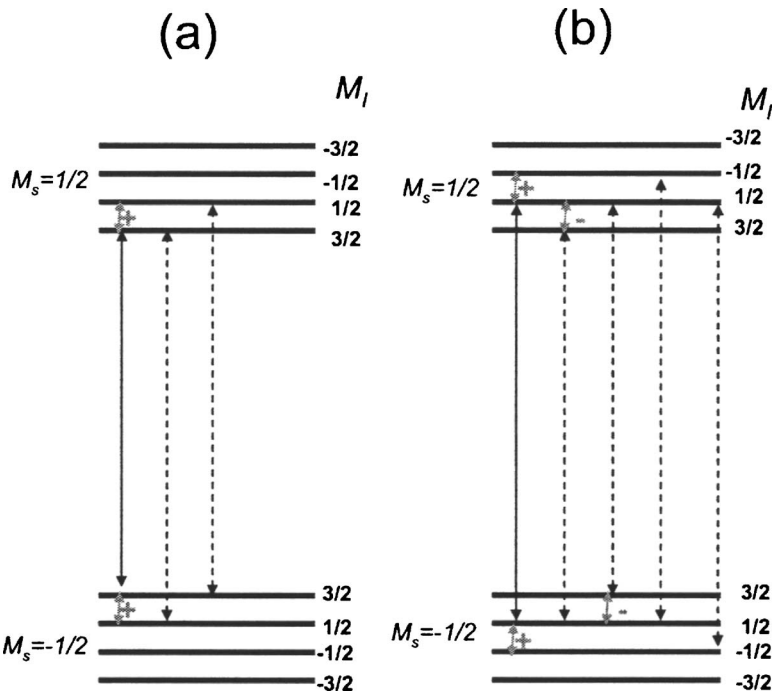

FIG. 7. A scheme of the electron and nuclear sublevels for a Cu-nucleus coupled to one electron. Solid lines depict the observer transition ν_{det}. Dashed lines represent the forbidden transition excited by the HTA pulse. (a) ν_{det} is set to the $M_I=\frac{3}{2}$ allowed transition and signals in ELDOR-detected NMR spectrum appear in positive region, $\Delta\nu=\nu_{HTA}-\nu_{det}>0$. (b) ν_{det} is set to the $M_I=\frac{1}{2}$ allowed transition and signals in ELDOR-detected NMR spectrum will appear at $\Delta\nu<0$ and $\Delta\nu>0$.

on different sides of the ELDOR-detected NMR spectrum. Indeed, comparison of the two sides, shown in Fig. 6(b), reveals peaks at different positions. Moreover, some lines that appear in the ELDOR-detected NMR spectrum cannot be found in the ENDOR spectrum; these could be attributed to $\Delta M_I=\pm 2$ transitions. Here, we do not attempt to analyze the full spectrum, but rather identify and assign the ^{63}Cu lines of the major quartet in the ED-EPR spectrum, to be used in the THYCOS experiment.

In principle, the THYCOS experiment may also generate spectral features arising from hyperfine-selective ENDOR type of experiment[7] due the similarity of the pulse sequences. In this experiment, which is based on the excitation of allowed EPR transitions only, a change in the echo/FID intensity occurs when $\Delta\nu=A$. In order to avoid such undesired effects, the correlation of the ^{63}Cu NMR lines in ELDOR-detected NMR and ^{1}H lines in ENDOR dimension was chosen. The ^{1}H ENDOR spectrum shows that the hyperfine splitting of the protons does not exceed 10 MHz, whereas ^{63,65}Cu signals are expected in the frequency range $\Delta\nu>50$ MHz, which is much larger than the largest hyperfine coupling exhibited by the protons.

The THYCOS spectra obtained with the HTA pulse set to $\Delta\nu=49.6$ and 120.5 MHz, are shown in Fig. 8 together with the ^{1}H ENDOR spectrum. Indeed, each THYCOS spectrum shows only one component of each ^{1}H doublet, and together they constitute the full ENDOR spectrum of the Cu^{2+} site(s) excited by the HTA pulse. The THYCOS spectra are further compared with the difference TRIPLE spectra, since they provide similar correlations. In the difference TRIPLE experiment, Fig. 2(b), the final spectrum is obtained by subtracting spectrum recorded without the first RF_1 pulse (ENDOR spectrum) from the one obtained RF_1 pulse. While the THYCOS spectra show ENDOR lines originating from the opposite manifold of that excited by the HTA pulse, the difference TRIPLE experiment produces lines belonging to the same manifold. Therefore, the THYCOS spectrum obtained with $\Delta\nu=49.6$ MHz should be compared TRIPLE spectrum recorded with $RF_1=120.5$ MHz, and vice versa, as shown in Fig. 8. The comparison of the THYCOS and TRIPLE experiments shows that, as expected, the THYCOS experiment produces the expected correlations.

To substantiate the assignment of the ^{1}H ENDOR lines to their corresponding paramagnetic sites (I or II) a series of pulse ^{1}H–^{1}H TRIPLE experiments were carried out as well, with the RF_1 pulse set to a number of ^{1}H lines, confirming the results shown in Fig. 8(A). In addition, the VMT ENDOR experiment[19,20] was applied to determine explicitly which of ^{1}H lines belong to the α and β electron spin manifolds. This experiment is similar to the Davies ENDOR experiment, with the exception that a long delay t_{mix} is introduced after the RF pulse [see Fig. 2(a)]. In this experiment, the lines that belong to the electron spin α manifold invert as t_{mix} increases. The results are shown in Fig. 8(B). While this experiment does not distinguish between ENDOR lines belonging to different sites, as THYCOS and TRIPLE, it does provide their explicit manifold. The assignment of the lines, as determined from the THYCOS and VMT ENDOR, is marked on the ENDOR spectrum on Fig. 8(A). This now allows us to proceed and assign the ^{63}Cu peak at 49.6 MHz to the β-manifold and the 120.5 MHz line to the α-manifold, yielding a negative ^{63}Cu hyperfine coupling, $A_{Cu}=-150.1$ MHz, for site I. Quantum chemical calculations on CuHis yielded a negative A_{zz}.[24] In addition, single crystal EPR measurements gave $A_{zz}=-395$ MHz, the magnitude of which is at least twice larger than the other principal hyperfine values $A_{xx}=186$ MHz, $A_{yy}=93$ MHz (Ref. 22) and, therefore, orientations with negative hyperfine splittings are highly probable.

A closer look at the THYCOS spectrum with $\Delta\nu=49.6$ MHz reveals that weak lines from other Cu^{2+} sites appear, marked on the ENDOR spectra with filled triangles

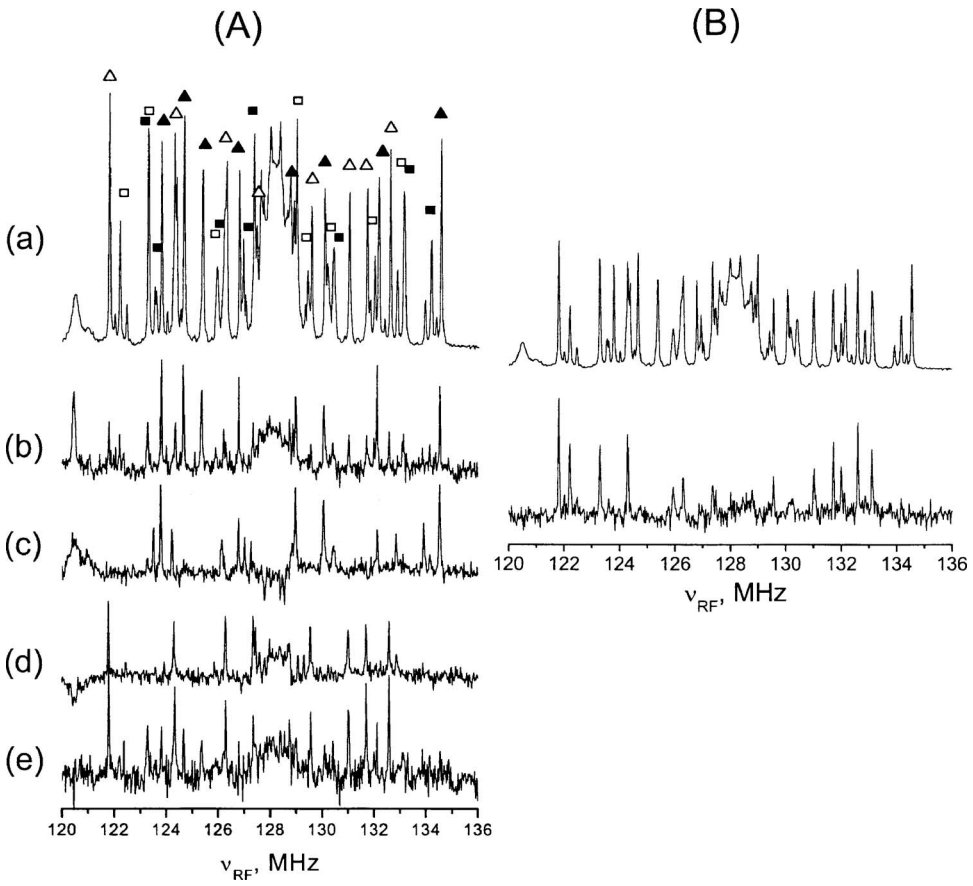

FIG. 8. (A) Spectra of a single crystal of Cu(II)-doped L-histidine: (a) Regular Davies ENDOR spectrum. Lines assignments: ▲—α-manifold of site I, △—β-manifold of site I, ■—α-manifold of site II; □—β-manifold of site II; [(b) and (e)] TRIPLE spectra recorded with RF pulse set to 120.5 and 49.8 MHz, respectively. [(c) and (d)] THYCOS spectra with HTA-pulse fixed on $\Delta\nu$=49.8 MHz and $\Delta\nu$ =120.5 MHz, respectively. (B) Comparison of the ENDOR spectrum with the VMT-ENDOR acquired with t_{mix} =1 ms.

and filled squares. Hence, at this experimental set-up the experiment is not completely selective in terms of the Cu^{2+} sites. The situation is worse in the case of the TRIPLE spectra. Nonetheless, it can be seen that the most significant contribution in the TRIPLE spectrum stems from site I and the lines that were affected by the selection of the Cu-line do belong to relevant manifold. The presence of the extra lines due to a second site suggests that the excited ^{63}Cu line (either by the HTA pulse in THYCOS and the first RF pulse in TRIPLE) is, in fact, a superposition of two lines. We attribute the better selectivity of the THYCOS spectra in this particular case to the partitioning of the signals between the positive and negative sides of the ELDOR-detected NMR spectrum as discussed above.

Frozen solution

The THYCOS experiment was also applied to a frozen solution of CuHis in D_2O. This is an orientationally disordered sample that exhibits an inhomogeneously broadened EPR spectrum due to the anisotropy of **g** and **A**. The ELDOR-detected NMR spectrum, measured at a field position corresponding to $g_\perp$, is depicted in Fig. 9. It shows a ^{2}H peak at 21.3 MHz, a ^{14}N doublet at 8 and 28 MHz, and a broad ^{65,63}Cu powder pattern between 40 and 90 MHz. Unlike for the single crystal spectrum showed above, here, the ELDOR-detected NMR spectrum is symmetric with respect to $\Delta\nu$=0 because the HTA pulse is not selective with respect to the M_I of ^{63,65}Cu due to the small $A_\perp$(Cu) and the inho-

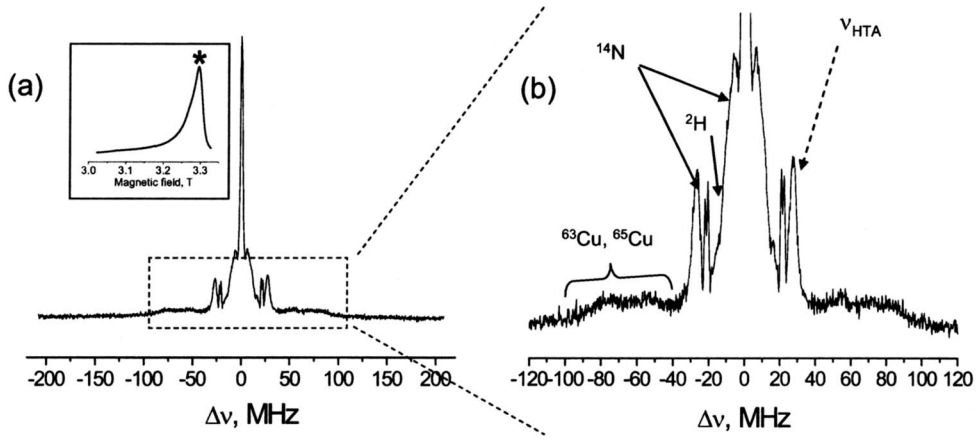

FIG. 9. (a) ELDOR-detected NMR spectrum of CuHis measured at 3.296 T, corresponding to $g_\perp$.(b) Expanded view of (a). The spectrum was recorded with t_{HTA}=2 μs, t_{det}=3 μs.

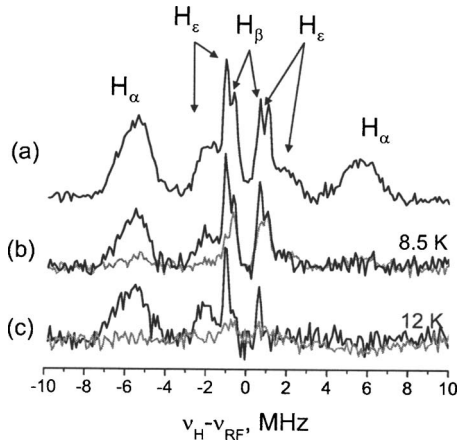

FIG. 10. The Davies ENDOR of spectrum of CuHis in a frozen solution of D_2O/per-deuterated glycerol, 8.5 K, along with the signals assignment. (b) and (c) THYCOS spectra with and without the HTA pulse (black and gray traces, respectively) recorded at 8.5 and 12 K.

mogeneous broadening induced by *g*-strain. CuHis has two inequivalently coordinated ^{14}N nuclei; $^{14}N_1$ and $^{14}N_2$ from the amino and imidazole groups, respectively [see Fig. 12(a)]. In single crystals of Cu(II)-doped L-histidine these ^{14}N nuclei have the following principal hyperfine values, $^{14}N_1$: $[A_{xx},A_{yy},A_{zz}]=[39.24,25.92,25.42]$ MHz, $^{14}N_2$: $[A_{xx},A_{yy},A_{zz}]=[37.7,29.3,28.5]$ MHz.[23] The signals of these two different ^{14}N nuclei are not resolved in the ELDOR-detected NMR spectrum of the frozen solution and the observed doublet corresponds to $A(^{14}N)=36$ MHz. Quadrupolar splitting are also not resolved. Considering that the width of the central hole is ~5 MHz, the differences between the two sets are below the resolution of the experiment. The ^1H Davies ENDOR of this complex is shown in Fig. 10(a) and the assignment of the signals, based on ^2H substitution,[16] are indicated in the figure.

The THYCOS sequence was applied with ν_{HTA} set to the ^{14}N line at $\Delta\nu=+28$ MHz [see Fig. 9(b)]. This line was chosen because it is intense and well separated from its counterpart. This spectrum [Fig. 10(b)], recorded at 8.5 K, is asymmetric as expected, and comprises signals belonging to only one M_S manifold, superimposed on weak residual ENDOR signals close to the ^1H Larmor frequency ν_H. Recording the spectrum without the HTA pulse reveals unexpected weak ENDOR signals [see Fig. 10(b)]. We attribute the presence of these residual ENDOR signals to incomplete relaxation of the nuclei during the time interval between consecutive sequences. Under a steady state, this would lead to a finite nuclear spin polarization at the beginning of a sequence, resulting in residual ENDOR signals.[25] These unwanted residual signals could be removed by increasing the temperature and, thereby, shortening the nuclear relaxation times, as shown by the THYCOS spectrum recorded at 12 K [Fig. 10(c)]. At this temperature, removal of the HTA pulse did not produce any spectrum.

The THYCOS experiment selected the low frequency component of H_α at −5.3 MHz, which interestingly, has the same width and shape as in the ENDOR spectrum. This indicates that the HTA pulse excited the full inhomogeneous ^{14}N peak without introducing additional orientation selection. This is attributed to the bandwidth of the hole created by the HTA pulse (see central hole), which is comparable to the width of the ^{14}N line. The +0.6 MHz signal of H_β appears in the THYCOS spectrum as well. More importantly, the experiment selected the complete M_S subpowder pattern of H_ε, ranging from −1 to −2 MHz. For comparison, the TRIPLE experiment is significantly more selective because of the small RF pulse bandwidth and, therefore, in order to record the full subpowder pattern both RF pulses have to be stepped in a 2D experiment, which is very time consuming.[5]

The signals appearing in the ^1H THYCOS spectrum belong to the M_S opposite that of the +28 MHz ^{14}N line. Furthermore, while the hyperfine splitting of H_α and H_ε have the same signs, as they appear to the left of ν_H [see Eq. (1)], H_β has a different sign. The absolute sign of the hyperfine coupling of H_α has been determined earlier by VMT ENDOR and was found to be positive.[19] Hence, the H_α signal appearing in the THYCOS spectrum corresponds to the α manifold and, therefore, the 28 MHz ^{14}N line belongs to the β manifold, yielding a positive hyperfine coupling. This is in accord with prediction from quantum chemical calculations which gave positive principal hyperfine values for both $^{14}N_1$ and $^{14}N_2$.[24] Furthermore, the +0.6 MHz line of H_β and the H_ϵ lines at −1.0 and −2.0 MHz also belong to α manifold. This yields a negative coupling for H_β and positive couplings to the H_ϵ singularities.

The possibility to extract the M_S sub-powder pattern of H_ϵ is particularly important in light of the proximity of its signals to ν_H. In this region, there is a large ambiguity re-

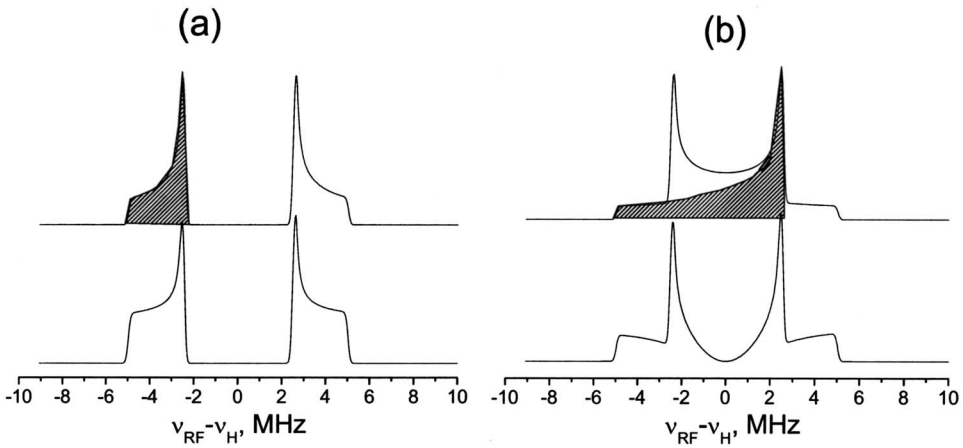

FIG. 11. Calculated ^1H ENDOR powder patterns (including all possible orientations relative to the external magnetic field) without (top) and with (bottom) the suppression hole for $t_p=300$ ns for (a) a proton with $A_\perp=5$ MHz and $A_\parallel=10$ MHz, and (b) $A_\perp=-5$ MHz and $A_\parallel=10$ MHz. The shaded areas mark the subspectrum of the $M_S=1/2$ (α) manifold.

garding the ENDOR line shape either owing to overlap with a signal from matrix protons and/or due to the amplitude attenuation of ENDOR signals acquired with the Davies ENDOR sequence. The latter arises from the so-called hyperfine contrast selectivity.[26] There, the ENDOR effect reduces to zero for hyperfine couplings $A<1/t_p$, where t_p is the length of the first selective MW pulse. This ambiguity reduces the uniqueness of hyperfine tensor components determined by spectral simulations. This problem is demonstrated in Fig. 11, which depicts calculated ^{1}H ENDOR powder patterns (including all possible orientations relative to the external magnetic field) for a proton at W band (ν_H=140 MHz) with $A_\perp$=−5 MHz and $A_\parallel$=10 MHz, where the subspectra of the $M_S=\pm 1/2$ overlap, and a protons with $A_\perp$=5 MHz and $A_\parallel$=10 MHz, where the subspectra do not overlap. The singularities of the two powder patterns appear in the same position, but they differ significantly in the region near ν_H. These are then compared with spectra calculated taking into account the suppression hole for t_p=300 ns. Now, the differences between the two are less prominent and in the presence of noise and broader lines, it would be difficult to distinguish the two without knowing the relative signs of $A_\perp$ and $A_\parallel$. Obviously, the presence of the distant matrix protons will complicate this further.

The principal values of $\mathbf{A}(H_\epsilon)$ and their orientation relative the g-tensor frame were determined earlier from simulations of orientation selective ^{1}H ENDOR spectra of CuHis-α, β_2-d_3 in D_2O/glycerol.[16] In these spectra, the region around ν_H was masked due to the presence of the signals of ^{1}H matrix protons from the nondeuterated glycerol present in the solution and of H_δ signals appearing close to ν_H. Therefore, only the region with $|\nu_{RF}-\nu_H|>1$ MHz was fitted in the simulations, and the line shape was simulated under the assumption that the peaks at −1.0 and −2.0 MHz belong to different M_S, namely, $A_{zz}>0$, $A_{yy,xx}<0$, because it was expected that the isotropic hyperfine coupling will be negligible. The THYCOS experiment, however, shows that the above choice turned out to be wrong. Now, with the known signs of the hyperfine splitting measured at $g_\perp$, we have simulated again the orientation selective spectra reported by Manikandan *et al.*,[16] and the results are shown in Fig. 12(b). The experimental ENDOR spectra become more asymmetric as the field approaches $g_\parallel$ and the line shapes become highly distorted, rendering their simulations rather difficult. Accordingly, the simulations concentrated mainly on the position of the outer edges of spectra recorded at the lower fields. The distortion/asymmetry is the consequence of the saturation of the NMR transitions.[19] The new values obtained are $[A_{xx},A_{yy},A_{zz}]=[0,2.5,5.5]$ MHz with Euler angles $\alpha=5°$, $\beta=65°$ with respect to the orientation of **g**. The earlier values were $[A_{xx},A_{yy},A_{zz}]=[\mp 1.0,\mp 2.4,\pm 5.4]$ MHz and $\alpha=0°$, $\beta=70°$. Density functional theory calculations predicted for H_ε $[A_{xx},A_{yy},A_{zz}]=[-1.04,0.0,4.97]$ MHz.[24]

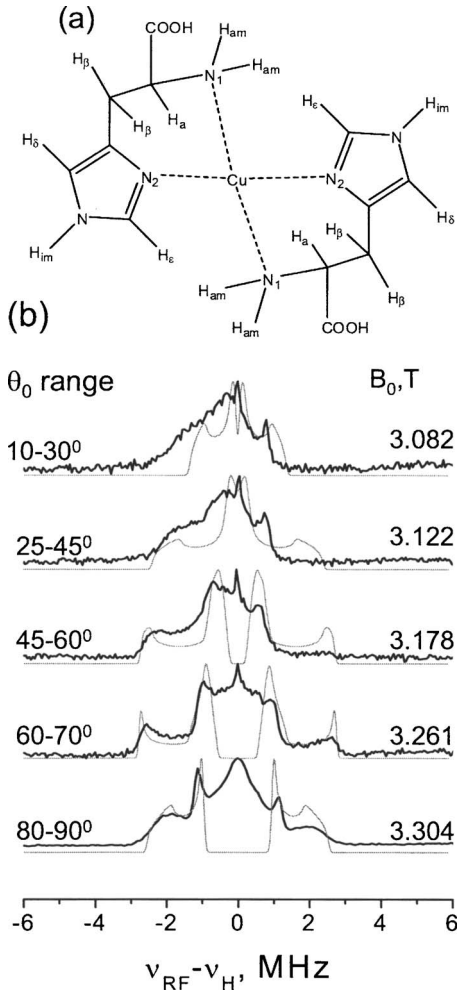

FIG. 12. a) The Davies ENDOR of spectrum of CuHis-d_3/D_2O/glycerol measured at different field positions within EPR spectra (black trace) (Ref. 16). The numbers next to each spectrum represent the angle between $g_\parallel$ and the direction of the external magnetic field. Gray traces correspond to new simulations with parameters given in the text. The simulations were carried out using the Easyspin MATLAB package (Ref. 28).

DISCUSSION

The new THYCOS experiment correlates ELDOR-detected NMR and ENDOR lines that belong to different M_S manifolds. The feasibility of the experiment has been demonstrated for a single crystal of Cu(II) L-histidine and for a Cu(II) bis-histidine complex in a frozen solution of water/glycerol. Because THYCOS is the combination of two experiments—ELDOR-detected NMR and ENDOR—it obviously features the characteristics of both. Namely, it is more effective at high fields and it has poor resolution in the ELDOR dimension. The resolution and sensitivity depend both on the experimental settings and relaxation times of the spin system. As it was mentioned before, the resolution is determined by T_m and, therefore, it features the same resolution as two-pulse ESEEM. Compared to the TRIPLE experiment, which yields the same type of information, it will always exhibit inferior resolution in the ELDOR dimension. However, the limited resolution in the ELDOR dimension could be sufficient for samples with an inhomogeneous linewidth larger than $1/T_m$. Moreover, sometimes the resolution can be sacrificed for the sake of sensitivity. When THYCOS is performed as a 1D experiment with the RF being swept, it is advantageous over TRIPLE for broad signals of low γ nuclei, such as ^{14}N. This is because the latter are not easily detected by ENDOR at a high field due the low hyperfine

enhancement factor[27] but are readily observed with ELDOR-detected NMR. Furthermore, the THYCOS experiment, as presented here, has the advantage that it is not a difference experiment and the resulting spectrum is immediately observed, as opposed to TRIPLE which requires subtraction of the ENDOR spectrum. The low resolution and the broad bandwidth can also be an advantage because it allows selecting of a complete sub-powder spectrum in one experiment as we have shown for CuHis. Another method that selects ENDOR lines according to their M_S origin is the VMT ENDOR. This method provide the absolute sign of the hyperfine splitting, and not only the relative sign, but it does not distinguish different sites. Moreover, contributions of the two M_S usually appear in the spectrum and consequently the lineshapes are complex, and the experiment works only for cases where the cross relaxation is much longer than the electron spin lattice relaxation time.[19]

The technical limitation of the THYCOS experiment is the bandwidth of the cavity. The critically coupled cylindrical single mode TE_{011} cavity used here has a bandwidth of about 100 MHz. This, however, does not imply that lines beyond the bandwidth cannot be observed, since overcoupling of the cavity and/or applying stronger pulses allows overcoming this. An obvious advantage of the experiment is that it does not require high MW power; for the HTA pulse, the output power of the bridge was 70 mW, which is available now with commercial spectrometers. A limitation of the experiment is the FID detection, which is necessary for optimum resolution but limits sensitivity.

CONCLUSIONS

A new triple resonance experiment, THYCOS, which correlates nuclear frequencies according to their respective paramagnetic site and specific M_S manifold, has been presented. The experiment can help resolving congested spectra, as often encountered in ^{1}H ENDOR spectra, and extract M_S sublevel powder pattern through correlations with another coupled nucleus that has a large hyperfine coupling and a strong signal in the ELDOR-detected NMR spectrum.

ACKNOWLEDGMENTS

This research has been supported by Binational USA-Israel Science Foundation (BSF). D.G. holds the Erich Klieger Professorial Chair in Chemical Physics. This research is made, in part, possible by the historic generosity of the Harold Perlman Family.

[1] P. Höfer, A. Grupp, H. Nebenführ, and M. Mehring, Chem. Phys. Lett. **132**, 279 (1986).
[2] R. J. Cook and D. H. Whiffen, Proc. Phys. Soc. London **84**, 845 (1964).
[3] M. Mehring, P. Höfer, and A. Grupp, Ber. Bunsenges. Phys. Chem. **91**, 1132 (1987).
[4] B. Epel and D. Goldfarb, J. Magn. Reson. **146**, 196 (2000).
[5] D. Goldfarb, B. Epel, H. Zimmermann, and G. Jeschke, J. Magn. Reson. **168**, 75 (2004).
[6] P. F. Liao and S. R. Hartmann, Phys. Rev. B **8**, 69 (1973).
[7] H. Thomann and M. Bernardo, Chem. Phys. Lett. **169**, 5 (1990).
[8] T. Wacker and A. Schweiger, Chem. Phys. Lett. **186**, 27 (1991).
[9] G. Jeschke and A. Schweiger, Chem. Phys. Lett. **246**, 431 (1995).
[10] G. Bar, A. Pöppl, S. Vega, and D. Goldfarb, J. Magn. Reson. **145**, 115 (2000).
[11] P. Schosseler, T. Wacker, and A. Schweiger, Chem. Phys. Lett. **224**, 319 (1994).
[12] T. Wacker, G. A. Sierra, and A. Schweiger, Isr. J. Chem. **32**, 305 (1992).
[13] S. V. Doorslaer and E. Vinck, Phys. Chem. Chem. Phys. **9**, 4620 (2007).
[14] L. Kulik, B. Epel, J. Messinger, and W. Lubitz, Photosynth. Res. **84**, 347 (2005).
[15] J. J. Shane, P. A. A. W. Van der Heijden, E. J. Reijerse, and E. de Boer, Appl. Magn. Reson. **6**, 427 (1994).
[16] P. Manikandan, B. Epel, and D. Goldfarb, Inorg. Chem. **40**, 781 (2001).
[17] I. Gromov, V. Krymov, P. Manikandan, D. Arieli, and D. Goldfarb, J. Magn. Reson. **139**, 8 (1999).
[18] B. Epel, I. Gromov, S. Stoll, A. Schweiger, and D. Goldfarb, Concepts Magn. Reson., Part B **26B**, 36 (2005).
[19] B. Epel, P. Manikandan, P. M. H. Kroneck, and D. Goldfarb, Appl. Magn. Reson. **21**, 287 (2001).
[20] B. Epel, A. Pöppl, P. Manikandan, S. Vega, and D. Goldfarb, J. Magn. Reson. **148**, 388 (2001).
[21] B. Epel, D. Arieli, D. Baute, and D. Goldfarb, J. Magn. Reson. **164**, 78 (2003).
[22] R. Hirasawa and H. Kon, J. Chem. Phys. **56**, 4467 (1972).
[23] C. A. McDowell, A. Naito, D. L. Sastry, Y. U. Cui, K. Sha, and S. X. Yu, J. Mol. Struct. **195**, 361 (1989).
[24] D. Baute, D. Arieli, F. Neese, H. Zimmermann, B. Weckhuysen, and D. Goldfarb, J. Am. Chem. Soc. **126**, 11733 (2004).
[25] T.-C. Yang and B. M. Hoffman, J. Magn. Reson. **181**, 280 (2006).
[26] C. Fan, P. E. Doan, C. E. Davoust, and B. M. Hoffman, J. Magn. Reson. **98**, 62 (1992).
[27] C. Gemperle and A. Schweiger, Chem. Rev. (Washington, D.C.) **91**, 1481 (1991).
[28] S. Stoll and A. Schweiger, J. Magn. Reson. **178**, 42 (2006).